A Power Takeoff Device for a Small Marine Hydrokinetic Turbine Deployed from an Unmanned Floating Platform

Hugo Pimentel, Adriana McKinney, Edward Henderson, John Frankenfield, Pierre-Philippe Beaujean, Manhar Dhanak*
Department of Ocean and Mechanical Engineering,
Florida Atlantic University
Boca Raton, USA
hpimentel2022@fau.edu, dhanak@fau.edu

***Abstract*— The design, development, and field-testing of a power takeoff (PTO) device equipped with a ball-type continuously-variable transmission (B-CVT) for a small marine hydrokinetic (MHK) turbine deployed from a floating unmanned autonomous mobile catamaran platform is described. The turbine is a partially-submerged multi-blade undershot waterwheel (USWW). The objective is to develop a PTO for the optimal conversion of the MHK energy harnessed by the turbine to electric power, which is stored in battery banks onboard the MHK platform. Modeling, simulation, and bench testing of the USWW and PTO show the feasibility of utilizing the B-CVT's variable gear ratio to decouple the USWW and generator speeds, maintaining the waterwheel within its optimal tip speed ratio (TSR) while varying the generator speed, thereby increasing the efficiency of the PTO. Results of bench and field testing in support of characterizing the power conversion capabilities of the PTO are described. The system being developed is in support of potential self-powered autonomous mobile recharge stations for unmanned aerial vehicles (UAVs) operating in coastal zones. Field tests of the complete MHK platform with 9 blades on the waterwheel and wheel submergences of 10 and 12 inches (full blade submergence) were performed. The overall proof-of-concept was successfully demonstrated, with the system satisfactorily capturing and converting water flow energy into electricity. The feasibility of utilizing the B-CVT as a means of increasing the PTO power capture capabilities and efficiency is analyzed.**

Keywords—renewable energy; marine hydrokinetic turbine; autonomous; PTO; USV; B-CVT

I. INTRODUCTION

As the transition to low-carbon economies takes place, consideration of efficient renewable energy technologies to not only increase power production but to drive cost down is of likely importance. Maximizing power production and operation time is not only important from an engineering perspective but also from an economical perspective, as it allows systems like the one discussed here to be economically viable and attractive, creating more competitive, cutting-edge solutions for renewable energy technologies, in turn contributing to the growth of the sector as a whole. Here, we describe a novel system, involving a marine hydrokinetic (MHK) turbine onboard an autonomous unmanned surface vehicle (USV) platform, that has been developed in support of potential remote coastal monitoring efforts. The USV is a 16ft Wave Adaptive Modular Vehicle (WAM-V) equipped with a flight deck for launch, recovery, and recharging of aerial drones, and with self-anchoring capabilities. The system is designed for deployment in 0.5 – 1m/s tidal, ocean or river currents to harness power from the water flow and trickle charge a battery bank onboard the USV. The USV consists of two inflatable pontoons and outboard electric thrusters and has capabilities for autonomous navigation. The MHK turbine consists of a Poncelet undershot waterwheel [1] with 9 curved blades and includes a flow accelerator designed to enhance the speed of the incoming flow (Fig. 1). The PTO consists of an input shaft driven by the USWW to a 35:1 gearbox, a ball continuously variable transmission (B-CVT) and a generator [2]. The B-CVT ratio ranges from 0.52 to 1.9 and is controlled via a servo motor, while speed measurements are taken by sensors placed on its input and output shafts. The battery charge controller (LT8491) manages power to the 12V lead-acid battery bank. The generator is the Freedom III Permanent Magnet Synchronous Generator (PMSG) rated at 1.5 kW at 970 rpm. The complete device is a prototype developed and tested at Florida Atlantic University (FAU).

The PTO consists of an input shaft driven by the USWW to a 35:1 gearbox, a ball continuously variable transmission (B-CVT), and a generator. The B-CVT ratio ranges from 0.52:1 to 1.9:1 and is controlled via a servo motor, while speed measurements are taken by sensors placed on its input and output shafts.

Fig. 1: WAM-V 16 USV-based MHK platform

979-8-218-14218-6 ©2023 MTS

The LT8491 battery charge controller manages power to the 12V lead-acid battery. The generator is the Freedom III Permanent Magnet Synchronous Generator (PMSG) rated at 1.5 kW at 970 rpm. The complete device is a one-of-a-kind prototype developed and tested at Florida Atlantic University (FAU).

II. PTO DESIGN AND TESTING

The overall PTO is comprised of several components, listed below and shown in Fig. 2. It is housed inside a cylindrical, water-resistant enclosure and contains seals on the input shaft to resist water penetration. Fig. 3 displays the housing location within the waterwheel.

1) *Input shaft from the waterwheel*
2) *Support disk*
3) *Planetary gearbox*
4) *B-CVT shift stack*
5) *B-CVT sub-system support*
6) *B-CVT transfer gears*
7) *NuVinci Ball CVT*
8) *Encoder plate and encoders*
9) *Generator*
10) *Support disk and structure mount*

Wherever possible custom-off-the-shelf (COTS) components were selected. The housing, component placement, and electronics were custom-made. The assembled PTO was bench tested in the laboratory using the setup [2].

A. Field Test Location and Procedures

Field-testing was conducted in the Intercoastal Waterway (ICW) located in Dania Beach, Florida, on two non-consecutive days, with different wheel submergences tested each day: 0.254 m (10 inches) on day 1 and 0.305 m (11 inches) on day 2.

For test purposes, the WAM-V was navigated via remote control to the assigned water resource location and anchored to the bottom at a location approximately 15ft deep as the tide transitioned from low to high tide. The goal was to capture peak water flow past the waterwheel. After successful anchoring, the waterwheel was deployed via an automated deployment system, and the behavior of the turbine was monitored.

The B-CVT was set to its minimum ratio to allow the wheel to gain speed and momentum. The B-CVT ratio was then increased, consequently leading to an increase in the generator speed and voltage.

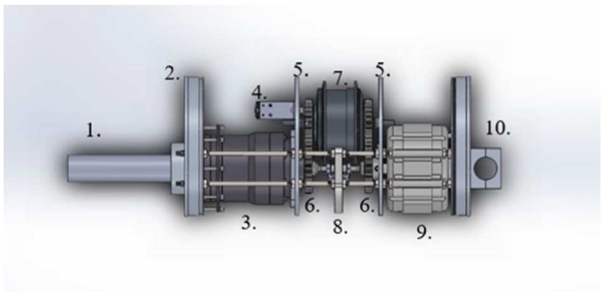

Fig. 2: The PTO components

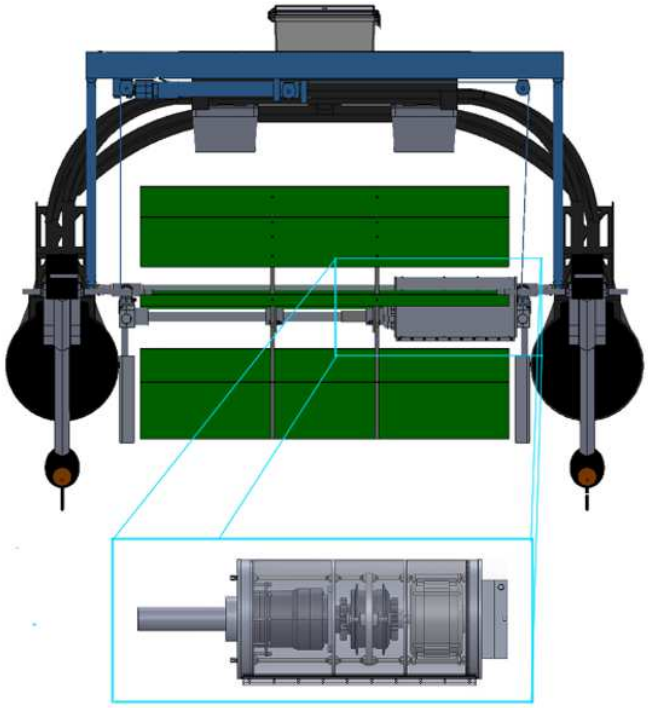

Fig. 3: The PTO housing onboard the USV

Since the effects of the charge controller on the system were unknown, the charge controller could be turned on and off remotely. In addition, the charge controller has an auto power-off feature when input voltages drop below its lower limit.

The final set of data collected during testing was: flow speed, generator voltage and current, B-CVT ratio, battery voltage and current, and charge controller status.

B. Issues During Tests

In the absence of sensors for recording rotational shaft speed and torque at the shaft, characterization of the generator and PTO under different speeds and electrical loads was performed to obtain mathematical models of those components. Using these models, it was possible to infer data not directly measured in the field tests from those measured during the tests. This technique does not replace proper measurements during tests and was only performed as an alternative to direct measurements, to make it possible to obtain more information about the performance of the system. Efforts are underway to install encoders for measuring shaft speed and sensors for recording torque generated.

C. Generator Model

First, the generator alone was characterized in the lab, where both generator speed and electrical resistance were varied and values for resistive torque and efficiency were computed. Fig. 4 shows the PTO and generator characterization setup on the test bench. A DC motor was used to vary the input speed and a 35:1 gearbox was used for speed multiplication.

The mathematical relationships for generator resistive torque and efficiencies were obtained as follows.

$$T_m = a_1(\mathrm{N})R^{b_1(\mathrm{N})} \quad (1)$$

The work is supported by the Dept. of Energy award DE-EE0008636.
USV development is supported by ONR under grant N000141812212.

$$\varepsilon_m = a_2(\mathrm{N})\ln(R) + b_2(\mathrm{N}) \quad (2)$$

$$a_1(\mathrm{N}) = -4\cdot 10^{-6}\mathrm{N}^2 + 0.0127\mathrm{N} - 0.794 \quad (3)$$

$$b_1(\mathrm{N}) = 1\cdot 10^{-6}\mathrm{N}^2 - 1.4\cdot 10^{-3}\mathrm{N} - 0.2143 \quad (4)$$

$$a_2(\mathrm{N}) = -7\cdot 10^{-7}\mathrm{N}^3 + 1\cdot 10^{-6}\mathrm{N}^2 - 7\cdot 10^{-4}\mathrm{N} - 5.12\cdot 10^{-2} \quad (5)$$

$$b_2(\mathrm{N}) = 4\cdot 10^{-9}\mathrm{N}^3 - 8\cdot 10^{-6}\mathrm{N}^2 + 4.5\cdot 10^{-3}\mathrm{N} + 0.2902 \quad (6)$$

where T_m is torque (Nm), ε_m is efficiency (%), R is electrical resistance (Ω), a_1, b_1, a_2, b_2 are speed-dependent coefficients and N is generator angular speed (rpm).

D. PTO Model

As with the generator torque and efficiency, a mathematical model for the overall PTO as a function of generator angular speed and electrical load was obtained, beginning on the input shaft and ending on the generator. The measured parameters for the PTO were the input shaft torque, the generator voltage, and the PTO total efficiency. A DC motor was used to vary the input speed to the PTO and a torque sensor was coupled to the input shaft for torque measurement. This time, a variable, programable load source was used so that a constant resistance could be maintained while the power varied.

Although voltage readings were available from field tests, the voltage model is necessary because it is modeled as a function of equivalent resistance (voltage divided by current, both available from field tests) and generator angular speed (not available during field tests). After obtaining that model, the mathematical relationship is solved for the angular speed, thus obtaining a model for the generator speed as a function of both voltage and equivalent electrical resistance. The model for the PTO output voltage is obtained as:

$$V_m = a_3(\mathrm{N})\,ln(R) + b_3(\mathrm{N}) \quad (7)$$

$$a_3(\mathrm{N}) = 0.002\mathrm{N} + 0.025 \quad (8)$$

$$b_3(\mathrm{N}) = 0.0433\mathrm{N} - 1.5383 \quad (9)$$

where V_m is voltage (Volts), and $a_3,\ b_3$ are speed-dependent coefficients.

By substituting the coefficients in the voltage model and solving for N:

$$\mathrm{N}_m = (V_m - 0.025\,ln(R) + 1.5383)/(0.002\,ln(R) + 0.0433) \quad (10)$$

Similarly, for the PTO input torque and efficiency,

$$T_{PTOm} = a_4(\mathrm{N})R^{b_4(\mathrm{N})} \quad (11)$$

$$\varepsilon_{PTOm} = a_5(\omega)\,ln(R) + b_5(\omega) \quad (12)$$

$$a_4(\mathrm{N}) = -8\cdot 10^{-6}\mathrm{N}^2 + 0.0129\mathrm{N} - 0.5782 \quad (13)$$

$$b_4(\omega) = 1\cdot 10^{-6}\mathrm{N}^2 - 1.2\cdot 10^{-3}\mathrm{N} - 0.017 \quad (14)$$

$$a_5(\mathrm{N}) = 3\cdot 10^{-7}\mathrm{N}^2 - 4\cdot 10^{-4}\mathrm{N} - 0.0209 \quad (15)$$

$$b_5(\mathrm{N}) = -2\cdot 10^{-6}\mathrm{N}^2 + 2.4\cdot 10^{-3}\mathrm{N} + 0.0674, \quad (16)$$

where T_{PTOm} is torque (Nm), ε_{PTOm} is mechanical efficiency (%), and $a_4,\ b_4,\ a_5,\ b_5$ are speed-dependent coefficients.

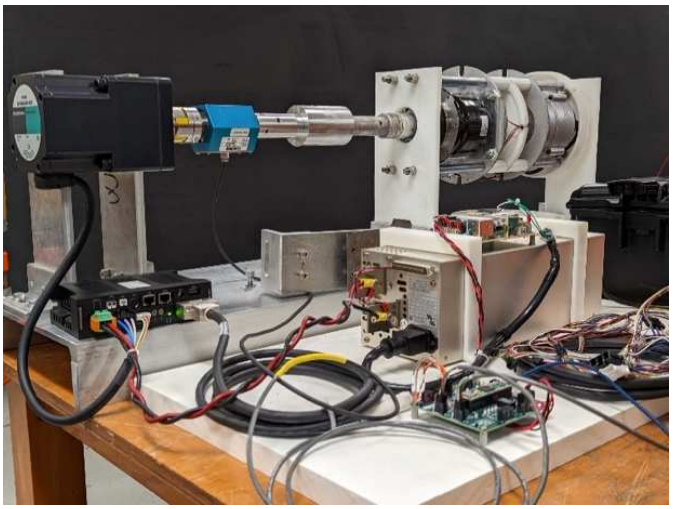

Fig. 4: The physical lab setup for generator and PTO characterization

E. Battery charge controller

The battery charge controller of the PTO was implemented using a COTS LT8491 battery charge controller evaluation board from Analog Devices. The default behavior of this device applies a fixed current to the battery during the constant-current portion of a lead-acid battery charge cycle. It maintains regulation of the current during the constant-current portion of the charge cycle (Stage 1) and limits the maximum charge current during the constant-voltage (Stage 2) portion as well. During field testing, the controller acted as a standalone system, without communication with the main PTO controller, except for input and output voltage and current readings.

III. FIELD TEST RESULTS

Field test results are presented here and are ordered beginning with data measured during testing (i.e., generator voltage, current, and power). Subsequently, the models obtained in the previous sections are applied to obtain further information regarding the performance of the PTO and the overall system. The data presented were filtered using a moving average filter with a window size of 200 samples.

Utilizing the dataset for generator output voltage and current obtained during the field test, it is possible to obtain the equivalent battery resistance dataset by dividing voltage by current. The electrical resistance is one of the independent variables of the models. The resistance dataset thus obtained is combined with the voltage output dataset to obtain the generator angular speed (RPM) dataset using Eq. 10. In turn the generator

speed and electrical resistance datasets thus determined are used to infer the other performance parameters using the previous models (Eq. 1-9).

Dividing the generator speed by the gear ratios, the waterwheel angular speed (RPM) can be obtained. Hence, the tip speed ratio (TSR) is obtained as $\mathrm{TSR} = 2\pi \mathrm{Nr}/60\mathrm{U}$, where r is the wheel radius (m). The generator torque is then obtained using Eq. 1. To infer the waterwheel power, the output electrical power is divided by the PTO total efficiency (Eq. 12), and to obtain the wheel torque, the power (W) is divided by the angular speed (rad s^{-1}). The PTO mechanical efficiency is obtained by dividing the total PTO efficiency by the generator efficiency. Lastly, for calculating the power coefficient (Cp), the flow power is obtained as

$$P_f = 1/2\rho A U^3, \tag{17}$$

where ρ is the water density (kg/m³), A is the cross-sectional area (m²) of the submerged blade section, and U (m/s) is the flow speed. Cp is then obtained as the ratio of the mechanical power of the waterwheel to the flow power.

A. Field Test 1 – 0.254 m Submergence

The field test conducted on Day 1 had higher flow speeds and yielded the highest levels of power generation and efficiency of both test days. Figs. 5, 6, and 7 show the generator output power, wheel Cp and TSR, and total system efficiency respectively for these tests. As previously mentioned, the models obtained in the last section allow for further investigation of the performance of the system.

B. Field Test 2 – 0.305 m Submergence

On Day 2, the tidal flow speeds were lower and correspondingly yielded lower levels of generated power and efficiency. However, it is important to evaluate the impact of varying flow speeds on the system. Figs. 8, 9, and 10 show the time series for generator output power, wheel Cp, TSR, and total system efficiency respectively. Once again, the models are applied here to obtain the additional data.

As mentioned before, some of the test results, which are performance indicators, were obtained from mathematical models of the generator and PTO. Those results, although they provide insightful information about the system's behavior and performance, have a certain degree of error due to the accuracy of models and bench-testing limitations. They do not substitute live data measurement and acquisition but were used as an alternative to the lack of sensors due to unforeseen circumstances. Therefore, the system's performance gives a limited, but good estimate of what it truly is and allows for conclusions to be drawn from experiments.

Table 1 summarizes the results from both test days.

TABLE I. SUMMARY OF TEST RESULT

	Test Day 1	***Test Day 2***
Submergence (m)	0.254	0.305
Avg Flow Speed (m/s)	1.06	0.91
Avg Power Output (W)	9.96	3.05
Avg Energy Output (W.h)	53.51	29.83
Avg Efficiency (%)	5.12	1.76

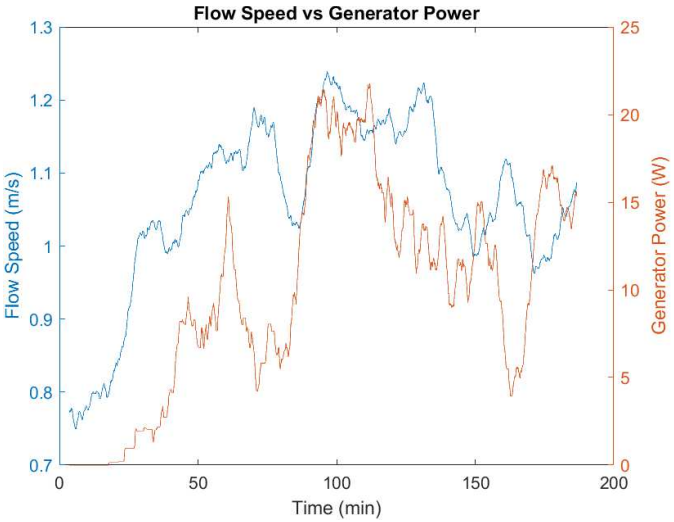

Fig. 5: Measured flow speed and associated electrical power output - day 1

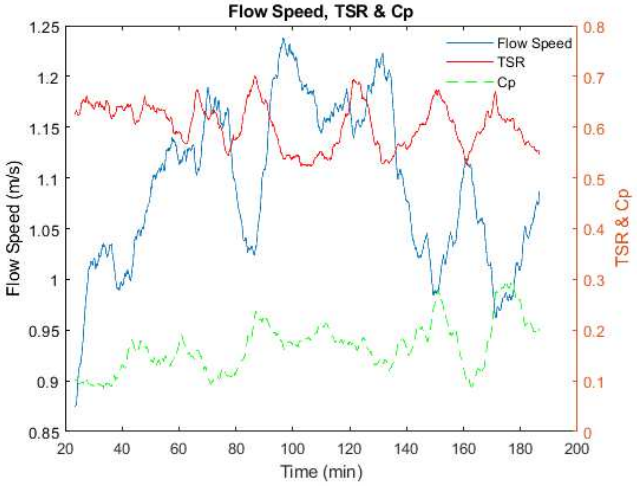

Fig. 6: Measured flow speed and associated turbine Cp and TSR - day 1

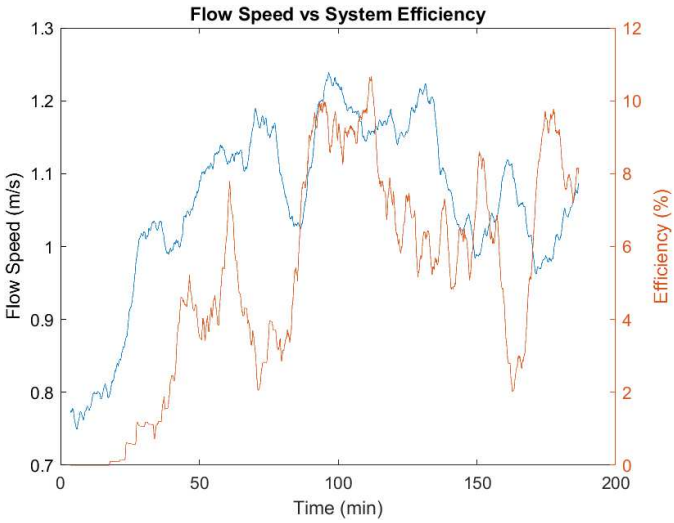

Fig. 7: Measured flow speed and associated system efficiency - day 1

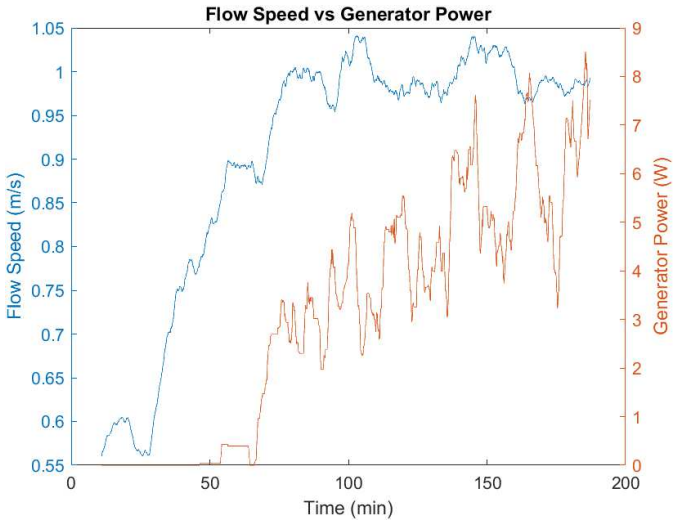

Fig. 8: Measured flow speed and associated electrical power output - day 2

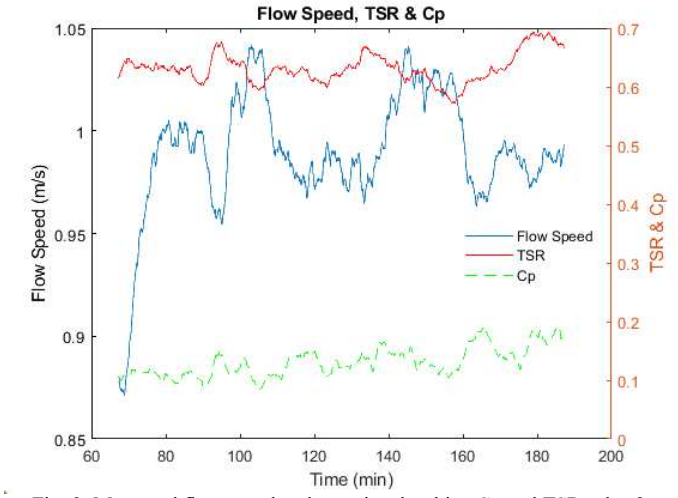

Fig. 9: Measured flow speed and associated turbine Cp and TSR - day 2

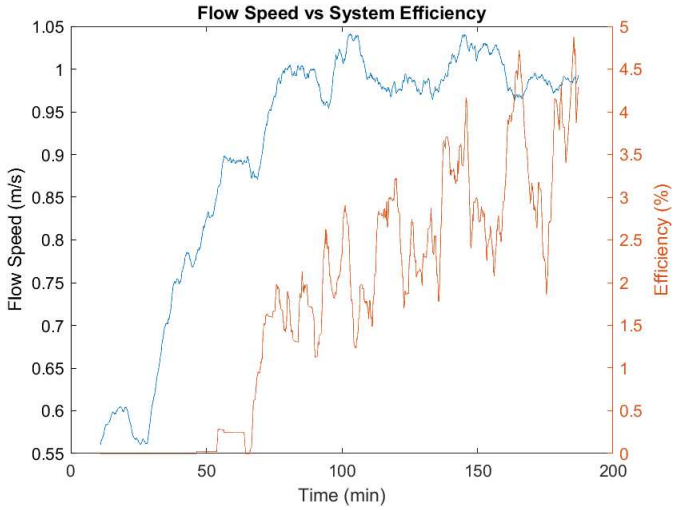

Fig. 10: Measured flow speed and associated system efficiency - day 2

C. Charge Controller

The main observation drawn from the tests is that the waterwheel operated outside of its optimal rpm range due to the lack of control of the charge controller. The first indication was the current demand spikes on the generator whenever the charge controller detected enough voltage, which caused a sudden load increase on the waterwheel, which in turn slowed it down drastically. That slowdown in turn decreased the total power being captured, which caused a drop in generator speed (therefore voltage) and forced the charge controller to disable itself. The charge controller had to be re-started once the generator voltage surpassed 10V, creating a cycle. However, although the cycle was completed during most of the tests, it did not happen all the time, as in certain cases the flow speed was high enough to keep the wheel momentum, which allowed the user to shift the B-CVT ratio higher to increase the generator RPM and generate more power. These events, however, only occurred at flow speeds of 1m/s and above. Fig. 11 shows the raw current demand data, controlled by the charge controller alone, during testing Day 2.

Furthermore, the PTO control system was not able to communicate with the charge controller and since the COTS charge controller has its own built-in, proprietary algorithm, there is no understanding of what that component is doing when controlling current. Proper communication and control need to be established between the PTO controller and the charge controller so that the current demand on the generator is effectively controlled, which relates to the torque load on the wheel being controlled and the system efficiency improved. Several papers [5-7] on wind turbines and torque control show the importance of controlling the torque in the system to achieve optimal operating points.

D. Generator

The generator specified and utilized in this study was rated at a speed and power far higher than what could be delivered, which leads to sub-optimal operation of the generator in the low-speed range. A generator rated for lower speed and torque is considered more suitable for the system.

To size such a generator, the flow power is obtained using Eq. 17. From the field data, with a maximum measured sustained flow speed measurement of 1.2 m/s, a cross-sectional area of 0.345 m² and a water density of 1000 kg/m³, the maximum power calculated from measurements is 298 W. Even though the limit for the Cp of a drag-based turbine, such as the USWW, is lower than that of a lift-based turbine (Betz limit), by assuming that the Betz limit of 0.56 for the lift-based turbines to apply, an estimate of the maximum power that can be captured by the waterwheel can be obtained as:

$$P_{ww} \approx 0.56\, P_f, \tag{18}$$

where P_{ww} is the waterwheel power (W).

Thus, the available power at the waterwheel at 1.2 m/s flow speed is estimated to be 167 W. Bench testing of the PTO yielded a maximum mechanical efficiency of 58%. The total power available at the generator input shaft is the product of the waterwheel power times the PTO mechanical efficiency, which gives 97 W of available input power to the generator. Therefore, a proper generator will be sourced based on the available power at its input shaft.

IV. CONCLUSIONS

Field-testing of a PTO equipped with a B-CVT for a small MHK turbine deployed from a floating unmanned autonomous mobile catamaran platform was successfully performed in support of characterizing the power conversion capabilities of the PTO. A proof-of-concept demonstration of the mobile unmanned surface vehicle MHK platform with the capability for power generation from renewable tidal currents was conducted, including the required tasks of automated turbine deployment from the platform, harnessing of power from the tidal current flow, electric power generation, and storage onboard the platform, PTO communication with an on-shore computer, and turbine and platform recovery. Work is underway to make the whole system significantly autonomous.

The data gathered allowed for performance and feasibility estimations of the prototype system. B-CVT ratio manipulation yielded an increase in generator speed and voltage output, and it showed the likelihood of performance improvements when properly controlled in tandem with the charge controller. The next steps will involve mainly the combination of those two devices under one controller to properly set their setpoints and optimize power production.

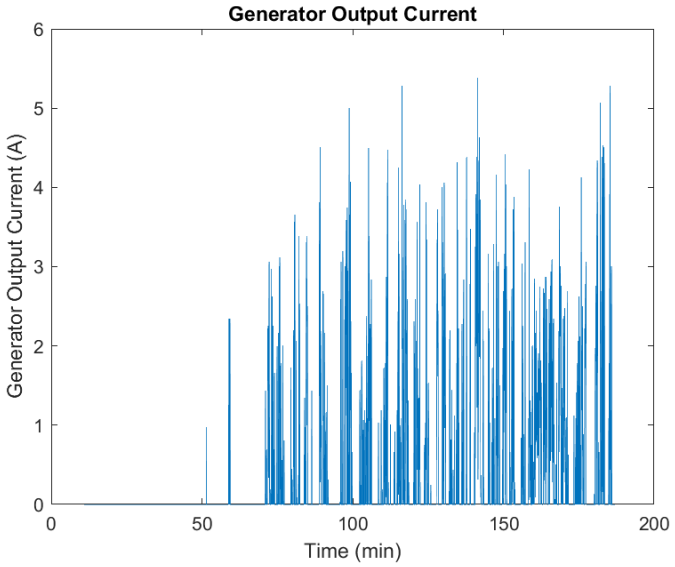

Fig. 11: Raw generator current demand - day 2

Based on the findings, a new 100W, 24V, low-torque, low-speed generator is being implemented that is expected to be more suitable for operations in expected tidal flow currents. Modifications to the charge controller are being implemented to allow the main PTO controller to better communicate with it and send current demand setpoint signals. A hardware modification to the LT8491 Evaluation Board is being designed, implemented, and tested that permits control of the charging current. A programmable voltage of 0 to 5 volts, developed by the PTO sub-system controller, will be applied to a filter and buffer amplifier. It is expected that a voltage change from 0 to 5 volts would result in a charge current change from the default charge current of 4 amps to approximately 0.4A respectively. The goal will be to have control over the torque load on the waterwheel so that it remains within its optimal TSR. The current demand control and the B-CVT ratio control would work in tandem to keep the waterwheel at its optimal speed and operate the generator at an optimal speed. The performance of the system will be determined through simulation under control laws that manipulate both control variables – B-CVT ratio and generator current demand – to keep the waterwheel within its optimal TSR setpoint. The goal is to find a good control strategy to maintain the system at its peak performance and deal with varying incoming flows. Models for the waterwheel flow-speed-torque, generator speed-torque-power, and charge controller dynamic behavior will be implemented in the simulation. A comparison between independent control of the B-CVT ratio and current demand versus optimized, tandem control of the B-CVT ratio and current demand will be run and results evaluated by measuring power output under both scenarios.

V. ACKNOWLEDGMENTS

The project is supported by the Department of Energy, USA under award DE-EE0008636. The development of the USV is being supported by the Office of Naval Research under grant N000141812212 (Program Manager: Kelly Cooper).

REFERENCES

[1] A. McKinney *et al*., "A Low-Flow Marine Hydrokinetic Turbine for a Floating Unmanned Mobile Platform," *OCEANS 2022, Hampton Roads*, Hampton Roads, VA, USA, 2022, pp. 1-6, doi: 10.1109/OCEANS47191.2022.9977141.

[2] E. Quaranta, R. Revelli, "Gravity water wheels as a micro hydropower energy source: a review based on historic data, design methods, efficiencies, and modern optimizations," Renewable and Sustainable Energy Reviews, Elsevier, vol 97(C), p. 414-427, 2018.

[3] Yonghun Yu, Junho Suh, Youngchan Ahn, "Performance evaluation of ball CVTs and comparison between conformal and non-conformal type, Mechanism and Machine Theory", Volume 156, 2021, 104139, ISSN 0094-114X, https://doi.org/10.1016/j.mechmachtheory.2020.104139.

[4] A. Hall, "Design, simulation, and testing of a B-CVT based PTO and controller for a small scale MHK-turbine in low flow speed operation," MSc Thesis, Dept. of Ocean & Mechanical Engineering, Florida Atlantic University, Boca Raton, FL, 2022.

[5] Kathryn Johnson, Lee Jay Fingersh, Mark Balas and Lucy Pao. "Methods for Increasing Region 2 Power Capture on a Variable Speed HAWT," AIAA 2004-350. *42nd AIAA Aerospace Sciences Meeting and Exhibit*. January 2004.

[6] Singh, J., & Ouhrouche, M. (2011). MPPT Control Methods in Wind Energy Conversion Systems. InTech. doi: 10.5772/21657

[7] Johnson, K. E. Adaptive Torque Control of Variable Speed Wind Turbines, report, (2004); Golden, Colorado. https://digital.library.unt.edu/ark:/67531/metadc1404940/.